Article ID: 1000-7032(2013)02-0123-10

Synthesis of $Sr_5(PO_4)_3Cl:Ce^{3+}$ Phosphors by Hydrothermal and Post-annealing Method

XIE Dong-hua, CHEN Xiang-ying*, CHEN Chong

(*School of Chemical Engineering, Anhui Key Laboratory of Controllable Chemistry Reaction & Material Chemical Engineering, Hefei University of Technology, Hefei* 230009, *China*)

* *Corresponding Author, E-mail: cxyhfut@gmail.com*

Abstract: A simple and efficacious hydrothermal and post-annealing method has been developed to prepare $Sr_5(PO_4)_3Cl:Ce^{3+}$ phosphors. The experimental results reveal that modulating the solvent species as well as the solvent composition (*i.e.* solvent effect) can give rise to $Sr_5(PO_4)_3Cl:Ce^{3+}$ phosphors with granular/rugby-like shapes and various sizes under hydrothermal conditions. The driving force for rugby-like $Sr_5(PO_4)_3Cl:Ce^{3+}$ phosphor growing along [001] direction originates from its intrinsic symmetry of $P6_3/m$. More importantly, post-annealing method was further carried out to investigate the luminescent properties of $Sr_5(PO_4)_3Cl:Ce^{3+}$ phosphors. Ce^{3+} doping content, calcination temperature, volume ratio in H_2O-triethyleneamine and two different synthetic methods play important roles in determining the emission intensity. The PL, PLE spectra and CIE chromaticity coordinates illustrate the excellent blue emission feature of $Sr_5(PO_4)_3Cl:Ce^{3+}$ phosphors.

Key words: $Sr_5(PO_4)_3Cl:Ce^{3+}$; phosphors; hydrothermal; solvent effect

CLC number: O6143.3; O625.5 **Document code**: A **DOI**: 10.3788/fgxb20133402.0123

利用水热-后煅烧方法制备 $Sr_5(PO_4)_3Cl:Ce^{3+}$ 磷光体

谢东华, 陈祥迎*, 陈 崇

(合肥工业大学化学工程学院 可控化学与材料化工安徽省重点实验室, 安徽 合肥 230009)

摘要: 利用一种简单有效的水热-后煅烧方法合成了 $Sr_5(PO_4)_3Cl:Ce^{3+}$ 磷光体。实验结果表明,通过调节水热条件的溶剂类型和组成可以得到球形/橄榄球形 $Sr_5(PO_4)_3Cl:Ce^{3+}$ 磷光体。橄榄球形 $Sr_5(PO_4)_3Cl:Ce^{3+}$ 磷光体的内在生长方向为[001],空间群为 $P6_3/m$。更为重要的是,可以利用后煅烧方法来研究 $Sr_5(PO_4)_3Cl:Ce^{3+}$ 磷光体的光学性能,发光强度的主要影响因素包括 Ce^{3+} 含量、煅烧温度、H_2O-三乙醇胺体系中的体积比。$Sr_5(PO_4)_3Cl:Ce^{3+}$ 磷光体的发光谱以及 CIE 色温图表明,该产物具有蓝光发射的特性。

关 键 词: $Sr_5(PO_4)_3Cl:Ce^{3+}$; 磷光体; 水热合成; 溶剂效应

收稿日期: 2012-11-20; **修订日期**: 2012-12-08

基金项目: 国家自然科学基金(21101052); 安徽省自然科学基金(090414194); 中国博士后科学基金(20100480045); 中央高校基本科研业务费专项资金资助项目

作者简介: 谢东华(1986-), 女, 安徽定远人, 主要从事光学、多孔炭材料的研究。
E-mail: 307645795@qq.com, Tel.: (0551)62901450

1 Introduction

Apatites and related compounds are of fundamental importance in several areas mainly including phosphor materials[1], laser hosts[2] and biocompatible materials[3]. They usually refer to hydroxylapatite, fluorapatite, chlorapatite and bromapatite, named for high concentrations of OH^-, F^-, Cl^- or Br^- ions, respectively. Especially, apatite type alkaline-earth halo-phosphates with general formula $M_5(PO_4)_3X$ (M = Ca, Sr, Ba) are outstanding as a family of phosphor host-matrix. For instance, $Ca_5(PO_4)_3(F,Cl):Sb^{3+}$, Mn^{2+} is the most important commercial white-emitting phosphor used in fluorescent lamps, in which the Mn^{2+} ion shows a broad-band orange emission and the energy transfer plays a central role[4]. Furthermore, blue-emitting chlorapatite phosphors doped with Eu^{2+}[5-7] applied in light emitting diodes (LED) have been extensively studied.

The Ce^{3+} with $4f^1$ electronic configuration undergoes 5d-4f transitions that are parity and electric dipole allowed transitions. The luminescent materials doped with Ce^{3+} efficiently absorb the excitation energy primarily in the ultraviolet (UV) region[8]. Up to now, except for the typical yellow-emitting $Y_3Al_5O_{12}:Ce^{3+}$ (YAG:Ce) phosphors, other kinds of phosphors doped with Ce^{3+} has been explored, including $Ba_2Ca(BO_3)_2:Ce^{3+}$[9], $CaSiN_2:Ce^{3+}$[10], $SrM_3SiO_5:Ce^{3+}$[11], *etc.* However, few reports was concerned on the Ce^{3+} activated apatites with the exception of $M_5(PO_4)_3F$ (M = Ca, Sr, Ba) under VUV-UV and X-ray excitation[12].

Apatite crystallographically has two types of cationic sites (M_I and M_{II}): the first type of site (M_I) locates at the centre of a slightly distorted tricapped trigonal prism constituted by nine oxygen atoms, corresponding to C_3 point group symmetry. The second type of site (M_{II}) is coordinated with six oxygen atoms of PO_4^{3-} network and one X^{-1} ion, with the local symmetry of C_{1h} point group[13]. Taking chlorapatite ($Sr_5(PO_4)_3Cl$) as an example, it is $P6_3/m$ crystal structure. Hence, apatite-based phosphors are expected to exhibit 1-D micro/nano-structures growing along c-axis. You *et al.*[14] adopted a hydrothermal method to fabricate $Sr_5(PO_4)_3Cl:Eu^{2+}$ nanorod bundles, which has blue emission.

Herein, $Sr_5(PO_4)_3Cl:Ce^{3+}$ phosphors have been prepared via a simple and efficacious hydrothermal and post-annealing method. The shapes and sizes of $Sr_5(PO_4)_3Cl:Ce^{3+}$ phosphors obtained under hydrothermal conditions were adjusted by altering the solvent species (pure H_2O, H_2O-ethylenediamine, H_2O-ethylene glycol, H_2O-N, N-dimethyl formamide) and volume ratio (pure H_2O, 3∶1, 1∶1, 1∶3) in H_2O-triethyleneamine. Ce^{3+} doping content, calcination temperature, volume ratio in H_2O-triethyleneamine and two different synthetic methods were adopted to investigate the luminescent properties of $Sr_5(PO_4)_3Cl:Ce^{3+}$ phosphors. Finally, various Commission Internationale de L'Eclairage (CIE) chromaticity coordinates (x, y) were achieved.

2 Experiments

2.1 Hydrothermal preparation of $Sr_5(PO_4)_3Cl:Ce^{3+}$ phosphors

In a typical procedure, $SrCl_2 \cdot 6H_2O$ (5 mmol), Na_2HPO_4 (3 mmol) and $Ce(NO_3)_3 \cdot 6H_2O$ (0.05 mmol) were in turn added into 40 mL distilled H_2O to form white suspension under magnetic stirring for 10 min in 50 mL autoclave Teflon-liner. In present experiment, to avoid the oxidation of Ce^{3+} into Ce^{4+} under hydrothermal conditions, 2 mL $N_2H_4 \cdot H_2O$ was also introduced. Next, mixed gas Ar-H_2 ($q_V(Ar):q_V(H_2)=80:20$) was pumped into the above solution for 20 min, which was further sealed in an stainless steel autoclave and kept at 120 ℃ in an electrical oven for 10 h. After that, the resulting white powder was filtered off, washed with distilled water and absolute ethanol for several times, and then dried under vacuum at 80 ℃ for 4 h.

A series of contrast experiments were conducted to prepare $Sr_5(PO_4)_3Cl:Ce^{3+}$ phosphors by adjusting the Ce^{3+} mole fraction (0.03, 0.05, 0.07, 0.10), solvent composition (pure H_2O, H_2O-EG, H_2O-DMF, H_2O-TEA) under hydrothermal conditions at 120 ℃ for 10 h.

Besides, some abbreviation words occurs in present work as follows: EDA = ethylenediamine; EG = ethylene glycol; TEA = triethyleneamine; DMF = N,N-dimethyl formamide.

2.2 Post-annealing $Sr_5(PO_4)_3Cl:Ce^{3+}$ phosphors

The as-obtained phosphors were further heated in a horizontal furnace under the protection of Ar gas at certain calcination temperature (400, 600, 800, 1 000 ℃) for 2 h to investigate their genuinely luminescent properties.

For comparison, bulk $Sr_5(PO_4)_3Cl:Ce^{3+}$ phosphors was obtained by a direct solid state method, in which $SrCO_3$, $(NH_4)_2HPO_4$, $SrCl_2 \cdot 6H_2O$ and CeO_2 acting as raw materials were heated at 1 000 ℃ for 2 h in Ar-H_2 ($q_v(Ar):q_v(H_2)=80:20$) gas.

2.3 Characterization

X-ray powder diffraction (XRD) patterns were obtained on a Rigaku Max-2200 with Cu Kα radiation. Field emission scanning electron microscopy (FESEM) images were taken with a Hitachi S-4800 scanning electron microscope. Transmission electron microscope (TEM) and high-resolution transmission electron microscope (HRTEM) images, and selected area electron diffraction (SAED) patterns were performed with a JEOL 2010 unit operated at 200 kV. X-ray photoelectron spectra (XPS) were obtained on a VG ESCALAB MK Ⅱ X-ray photoelectron spectrometer with an exciting source of Mg Kα (1 253.6 eV). Photoluminescent (PL) analysis was conducted on a Hitachi F-4500 spectrophotometer equipped with Xe lamp at room temperature.

3 Results and Discussion

The phase, crystallinity and purity of samples were characterized by XRD technique. In present work, certain amount of white powder appears in the autoclave Teflon-liner after hydrothermal treatment of $SrCl_2 \cdot 6H_2O$, $(NH_4)_2HPO_4$ and $Ce(NO_3)_3 \cdot 6H_2O$ at 120 ℃ for 10 h. The corresponding XRD pattern is shown in Fig. 1(a). Its diffraction peaks can be totally indexed as hexagonal $Sr_5(PO_4)_3Cl$ (JCPDS Card No. 16-0666). No obvious diffraction peaks for $SrHPO_4$ occurs in Fig. 1(a), which usually comes from solution with pH value below *ca.* 8 ~ 9[14]. Herein, the addition of $N_2H_4 \cdot H_2O$ can increase the pH value in solution, which makes the pH value up to *ca.* 9 ~ 10 even after the hydrothermal reaction. Several comparative experiments using H_2O-EDA, H_2O-TEA, H_2O-EG or H_2O-DMF ($v:v$ = 1:1) as mixed solvent were conducted. The resultant XRD patterns reveal that all the samples can also be assigned to hexagonal $Sr_5(PO_4)_3Cl$. It indicates that the solvent species have less impact on the phase of $Sr_5(PO_4)_3Cl$ sample. Furthermore, no diffraction peaks from cerium hydroxides or oxides appear in Fig. 1 because of their low content.

$Sr_5(PO_4)_3Cl$ sample prepared by hydrothermal treatment, then post-annealing strategy was adopted at 800 ℃ for 2 h in a flow of Ar gas. XRD pattern is revealed in Fig. 1(b). Comparing with JCPDS Card No. 24-1008, several diffraction peaks in hexagonal $Sr_3(PO_4)_2$ reveal the thermally unstable characteristics of $Sr_5(PO_4)_3Cl$. However, the present result based on XRD pattern is not well consistent with the previous reports, where chlorine substituted hydroxylapatites have thermal stability till 1 200 ℃[15].

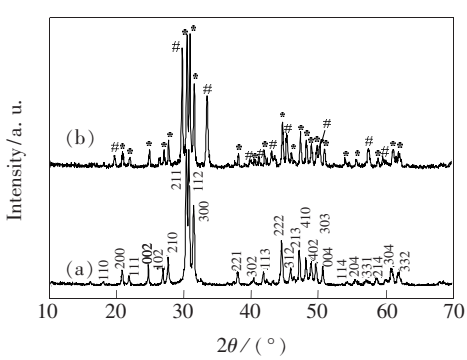

Fig. 1　XRD patterns of the samples obtained in pure H_2O under hydrothermal conditions at 120 ℃ for 10 h (a), and by post-annealing the above sample at 800 ℃ for 2 h in a flow of Ar gas(b). Notes: * = hexagonal $Sr_5(PO_4)_3Cl$ (JCPDS Card No. 16-0666); # = hexagonal $Sr_3(PO_4)_2$ (JCPDS Card No. 24-1008).

FESEM technique was employed to vividly depict the genuine sizes and shapes of $Sr_5(PO_4)_3Cl:Ce^{3+}$ samples obtained under hydrothermal conditions at 120 ℃ for 10 h. Considering the fact that the symmetry of apatite is $P6_3/m$, it typically forms

hexagonal crystals along *c*-axis, giving rise to nanorods[16] or nanowires[17]. Consequently, the present $Sr_5(PO_4)_3Cl:Ce^{3+}$ sample prepared in pure H_2O is expected to possess 1-D nanostructures. They are thus testified by the FESEM image and showed in Fig. 2(a). Additionally, the physicochemical solvent properties, such as polarity, viscosity, and surface tension, will strongly influence the solubility, stability and reaction rates. We chose EG, EDA and DMF as representative solvents to investigate the solvent effect on shapes and sizes of $Sr_5(PO_4)_3Cl:Ce^{3+}$ samples. In the case of mixed solvents of H_2O-EDA or H_2O-EG ($v:v=1:1$), large numbers of nanoscale particles appear, as shown in Fig. 2(b) and 2(c). In the case of mixed solvents of H_2O-DMF ($v:v=1:1$), 1-D nanorods coexisting with minor nanoparticles occur, as displayed in Fig. 2(d). Hence, altering the composition of mixed solvents can result in distinguishable nanostructures. In details, the presence of pure H_2O or H_2O-DMF is well propitious to the formation of 1-D nanostructures. The presence of H_2O-EDA or H_2O-EG can lead to isotropic growth towards $Sr_5(PO_4)_3Cl:Ce^{3+}$ samples.

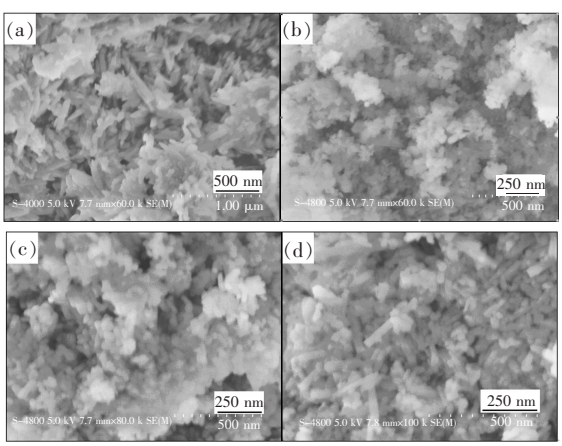

Fig. 2 FESEM images of the samples obtained in various mixed solvents ($v:v=1:1$) under hydrothermal conditions at 120 ℃ for 10 h. (a) Pure H_2O, (b) H_2O-EDA, (c) H_2O-EG, (d) H_2O-DMF.

To further investigate the solvent effect on the manipulation of $Sr_5(PO_4)_3Cl:Ce^{3+}$ samples, some parallel experiments were carried out in mixed solvents of H_2O-TEA under various volume ratios. In virtue of the magnified FESEM image shown in Fig. 3(a), uniform rugby-like shapes $Sr_5(PO_4)_3Cl:Ce^{3+}$ nanostructures emerge when using pure H_2O as single solvent. The lengths are up to ca. 300 ~ 400 nm. Interestingly, when adjusting the volume ratio of H_2O to TEA as 3∶1, rugby-like $Sr_5(PO_4)_3Cl:Ce^{3+}$ nanostructures up to *ca.* 200 nm appear, as is shown in Fig. 3(b), which are evidently smaller than that obtained in pure H_2O. Similar nanostructures in shapes/sizes also occur when further increasing the volume ratio of H_2O to TEA up to 1∶1 or 1∶3. It can thus be concluded that adding TEA into H_2O with designated volume ratio can markedly shorten the $Sr_5(PO_4)_3Cl:Ce^{3+}$ nanostructures in axial direction. The reason might originate from the solvent effect caused by the addition of TEA, which can induce the variation of solubility, stability and reaction rates in mixed solution.

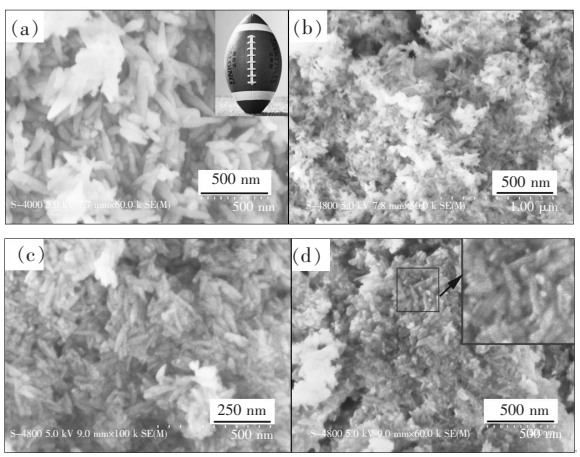

Fig. 3 FESEM images of the samples obtained in mixed solvents H_2O-TEA under hydrothermal conditions at 120 ℃ for 10 h. (a) Pure H_2O, (b) $v:v=3:1$, (c) $v:v=1:1$, (d) $v:v=1:3$.

The typical schematic diagram of $Sr_5(PO_4)_3Cl:Ce^{3+}$ nanostructures obtained in various solvents under hydrothermal conditions was illustrated in Fig. 4.

TEM, SAED, and HRTEM were used to further investigate the crystal structure and morphology of the as-prepared $Sr_5(PO_4)_3Cl:Ce^{3+}$ sample obtained in mixed solvents of H_2O-TEA ($v:v=1:1$) under hydrothermal conditions at 120 ℃ for 10 h. Fig. 5(a) gives us the panoramic view on this sample, which is mostly like the FESEM result depicted in Fig. 3(c). In addition, some of them remain the unique rugby-like nanostructures up to *ca.* 150 ~ 200

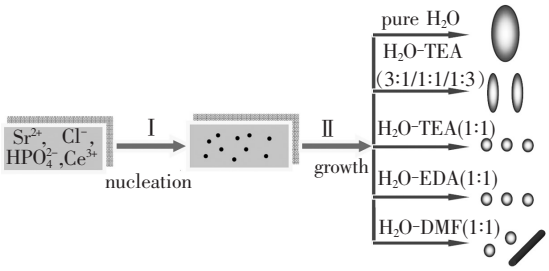

Fig. 4　Schematic diagram of $Sr_5(PO_4)_3Cl$: Ce^{3+} nanostructures obtained in various solvents under hydrothermal conditions. Notes: Once the raw materials as $SrCl_2 \cdot 6H_2O$, Na_2HPO_4 and $Ce(NO_3)_3 \cdot 6H_2O$ pre-dissolved in solution were added together, large quantity of white suspension forms immediately, indicating the occurrence of nucleation step. Next, various kinds of micro/nano-scale structures appear during the growth step under hydrothermal conditions, in which the solvent effect induced by the solvent species and solvent composition is believed to play a crucial role.

nm in length. To further give an insight into the crystal structure of $Sr_5(PO_4)_3Cl$: Ce^{3+} sample, HRTEM technique was adopted. Fig. 5(c) reveals the emblematical HRTEM image taken from an individual 1-D rugby-like nanostructure shown in Fig. 5(b). In virtue of the explicit lattice fringe and the fast Fourier transform (FFT) pattern in Fig. 5(c), we can discern that $Sr_5(PO_4)_3Cl$: Ce^{3+} nanostructure is single-crystal in nature and axially grows along [001] direction. Besides, the lattice spacing of 0.36 nm and 0.49 nm between adjacent lattice planes well correspond to those of (002) and (110) crystal planes of $Sr_5(PO_4)_3Cl$ sample. Fig. 5(d) is the corresponding SAED pattern with the crystal zone axis [001], which well complies with the HRTEM images shown in Fig. 4(c). It is also noteworthy that the $Sr_5(PO_4)_3Cl$: Ce^{3+} nanostructure is much electron-beam sensitive when conducting HRTEM observation. The crystal structure changes and some nanoscale holes occur, as illustrated in Fig. 5(c). This kind of low thermal stability $Sr_5(PO_4)_3Cl$: Ce^{3+} sample coincides well with the XRD result revealed in Fig. 1(b).

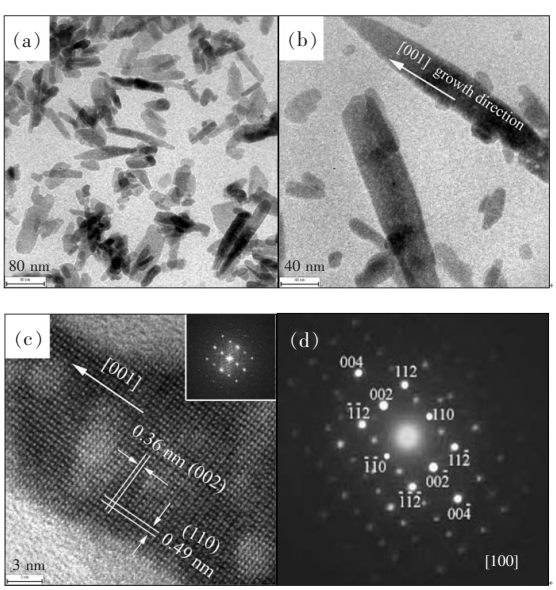

Fig. 5　(a ~ c) TEM and HRTEM images and (d) SAED pattern of the samples obtained in mixed solvents H_2O-TEA (v: v = 1: 1) under hydrothermal conditions at 120 ℃ for 10 h

The present 1-D nanostructure of $Sr_5(PO_4)_3Cl$: Ce^{3+} sample has the same growth direction along [001] as that of nanorod bundles assisted with the addition of ethylenediamine tetraacetic acid[14]. As we know, hexagonal crystal structure such as ZnO and CdS often shows the anisotropic growth characteristic along the [001] direction. It is therefore believed that the inherent driving force within $Sr_5(PO_4)_3Cl$: Ce^{3+} sample favors the preferential growth along *c* axis. Furthermore, the species of raw materials used herein as well as the kinetics parameters including concentration, pressure and temperature under hydrothermal conditions give rise to the formation of unique rugby-like nanostructures

X-ray photoelectron spectroscopy (XPS), serving as a typical quantitative spectroscopic technique, was conducted to measure the elemental composition, empirical formula, chemical state and electronic state of the elements that exist within $Sr_5(PO_4)_3Cl$: Ce^{3+} sample. The narrow-scan spectra of the XPS peaks of Sr, P, Cl, and Ce elements are given in Fig. 6. The Sr3d binding energies centered between 131.5 eV and 133.2 eV in Fig. 6(a), which are close to that of crystalline $SrTiO_3$ (132.10 eV)[18]. In addition, the binding energies for P2p in Fig. 6(b) are almost same to that of Sr3d, indicating the presence of PO_4^{3-} in sample[19]. As for the peak located at 197.5 eV in Fig. 6(c), it can be identified as Cl2p with the valence of -1[20]. The binding energies centered at 883.6 eV and 902.5

eV in Fig. 6(d) well accord with those of $Ce3d_{5/2}$ and $Ce3d_{3/2}$ spin-orbit doublet, revealing the electronic states of Ce^{3+} states in existence[21]. The XPS results prove that adding $N_2H_4 \cdot H_2O$ and the reducing gas (Ar-H_2) in sequence into solution before hydrothermal treatment can efficaciously protect the

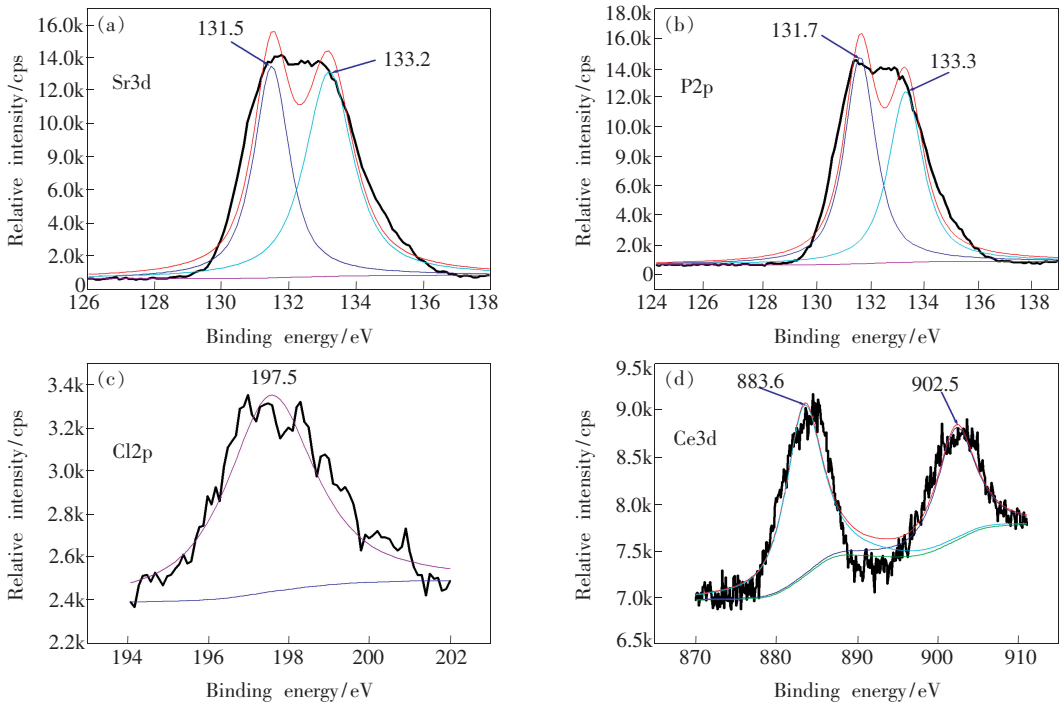

Fig. 6 XPS spectra of $Sr_5(PO_4)_3Cl$: Ce^{3+} sample obtained under hydrothermal conditions at 120 ℃ for 10 h in pure H_2O. (a) Sr3d, (b) P2p, (c) Cl2p, (d) Ce3d.

oxidation of Ce(Ⅲ) into Ce(Ⅳ) in sample.

The excitation and emission spectra were measured at room temperature to study the photoluminescent properties of $Sr_5(PO_4)_3Cl$: $0.01Ce^{3+}$ phosphors, as shown in Fig. 7. As is well known, the emission of Ce^{3+} ion has a typical d-f [$4f^05d^1 \rightarrow 4f^1(^2F_J)$] transition, as illustrated in the inset of Fig. 7, and commonly exhibits a broad emission peak. The excitation peak ranges from approximately 250 nm to 325 nm and shows a strong intensity centered at 284 nm (λ_{em} = 257 nm). Upon excitation at 284 nm, a broad emission peak ranging from approximately 315 nm to 435 nm occurs in Fig. 7, also possessing a doublet profile with maxima at 347 nm (3.57 eV) and 370 nm (3.36 eV), as fitted by Gaussian model. Such a property is the characteristic of Ce^{3+} luminescence, which definitely corresponds to the transitions from the 5d excited state to the $^2F_{5/2}$ and $^2F_{7/2}$ spin-orbitally split ground states of the 4f configuration[22]. Besides, the energy difference between 347 nm and 370 nm is 1 791 cm^{-1},

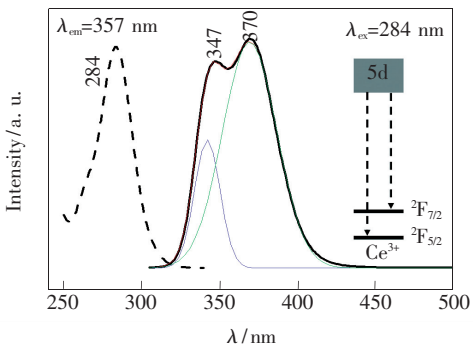

Fig. 7 The excitation (dashed line) and emission (solid line) spectra of $Sr_5(PO_4)_3Cl$: $0.01Ce^{3+}$ phosphors obtained at calcination temperature of 800 ℃ for 2 h in Ar gas. Notes: (1) Black line is the experimental results and green/red/blue lines are the Gaussian fitting results. (2) The inset is the typical energy level diagram of Ce^{3+} emissions.

which is close to the theoretical value of 2 000 cm^{-1}, demonstrating that there is only one type of Ce^{3+} luminescence center in the lattice[23].

Practically, concentration quenching of luminescence is an important phenomenon in all doped luminescent phosphors. The dopant materials

commonly suffer an effect of to avoid quenching at high doping content. It can lead to extensive reduction of the emission intensity and efficiency of the devices. Thus, a theory was presented for to avoid quenching in solid systems, based on the migration of excitation energy from one activator center to aother and eventually to an energy defect[24]. In present study, the concentration dependent emission spectra of $Sr_5(PO_4)_3Cl$: Ce^{3+} phosphors (monitored at 284 nm) with various Ce^{3+} doping content are shown in Figure 8. Apparently, the broad blue-emitting spectra from 300 nm to 450 nm are genuinely due to the d-f [$4f^05d^1 \rightarrow 4f^1(^2F_J)$] transition of Ce^{3+} ion, which has the maxima intensity centered at 362 nm. From the results in Fig. 8, we can clearly see that the PL intensity increases with dopant content of Ce^{3+} ion when $n < 0.05$. However, concentration quenching effect of Ce^{3+} ion occurs when $n > 0.05$. Accordingly, the optimal Ce^{3+} ion dopant content (n) is *ca.* 0.05 mol per formula unit.

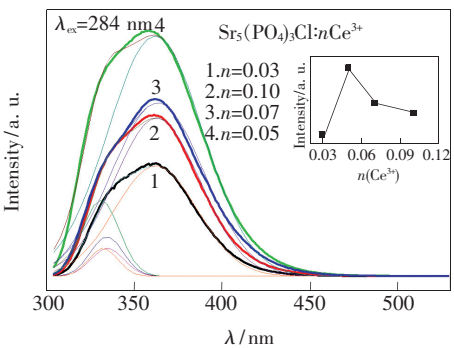

Fig. 8　The emission spectra of $Sr_5(PO_4)_3Cl$: Ce^{3+} phosphors with various Ce^{3+} doping content at calcination temperature of 800 ℃ for 2 h in Ar gas

We also conducted a series of temperature-dependent experiments to investigate the authentic impact of calcination temperature on the emission of $Sr_5(PO_4)_3Cl$: Ce^{3+} phosphors, as shown in Fig. 9. Higher crystallinity means higher ordered structure and less bulk defect which acts as a quenching site consuming excited photoelectrons without the radiation. The PL intensity gradually increase with the treatment temperature before the bulk crystal structure is destroyed. The PL intensity at 600 ℃ calcination temperature is much smaller than that at 800 ℃. The maximum PL intensity appears when designating the calcination temperature at 800 ℃ instead of 1 000 ℃ in Fig. 9. Similar phenomenon was also observed towards Eu^{3+}-doped Gd_2O_3 nanopowders[25]. As a consequence, the optimal calcination temperature for $Sr_5(PO_4)_3Cl$: 0.05 Ce^{3+} phosphors is 800 ℃.

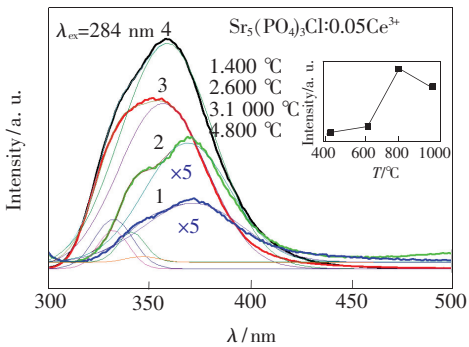

Fig. 9　The emission spectra of $Sr_5(PO_4)_3Cl$: Ce^{3+} phosphors with various calcination temperatures

On the other hand, because the volume ratios in mixed solvents of H_2O-TEA remarkably affect the shapes and sizes of $Sr_5(PO_4)_3Cl$: Ce^{3+} samples, as depicted in Fig. 3, we further carried out size-dependent experiments to investigate the composition in H_2O-TEA on the emission of $Sr_5(PO_4)_3Cl$: Ce^{3+} phosphors while keeping the Ce^{3+} ion dopant content as 0.05 and the calcination temperature as 800 ℃. Park and co-workers prepared $BaMgAl_{10}O_{17}$: Eu^{2+} phosphor particles by spray pyrolysis and found that the PL intensity has a linear relationship with the crystallite size. The crystallite size is critical variable affecting the PL intensity because larger crystallite size means more ordered structures and fewer bulk defects[26]. Herein, the PL intensity curves shown in Fig. 10 evidently indicate that the $Sr_5(PO_4)_3Cl$: Ce^{3+} phosphor obtained in pure H_2O is much higher that those obtained in mixed solvents in H_2O-TEA. It can be concluded that the larger the size, the higher the PL intensity, which is in good accordance with that of the $BaMgAl_{10}O_{17}$: Eu^{2+} phosphors above-mentioned.

To compare the effect of two different synthetic methods, *i. e.* solid-state method and the hydrothermal and post-annealing method, on the luminescent properties of the $Sr_5(PO_4)_3Cl$: Ce^{3+} phosphors, bulk $Sr_5(PO_4)_3Cl$: Ce^{3+} phosphors was prepared by

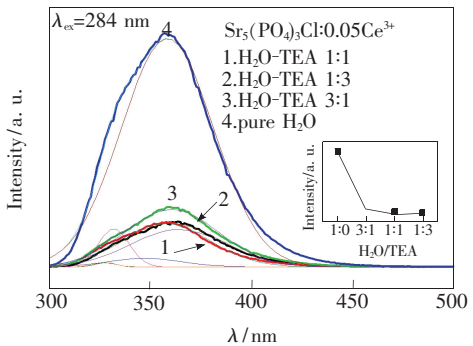

Fig. 10 The emission spectra of $Sr_5(PO_4)_3Cl:Ce^{3+}$ phosphors obtained at calcination temperature of 800 ℃ for 2 h in Ar gas with various volume ratios in mixed solvents of H_2O-TEA

a direct solid state method at 1 000 ℃ for 2 h under Ar-H_2 (q_V(Ar): q_V(H_2) = 80∶20) gas. The emission spectra are displayed in Fig. 11, in which both emission spectra are almost the same at 359 nm under the excitation of 284 nm. However, the PL intensity obtained by hydrothermal and post-annealing method is much higher than that obtained by conventional solid-state method. It is likely that the size effect contributes to the discrepancy of PL intensity[27].

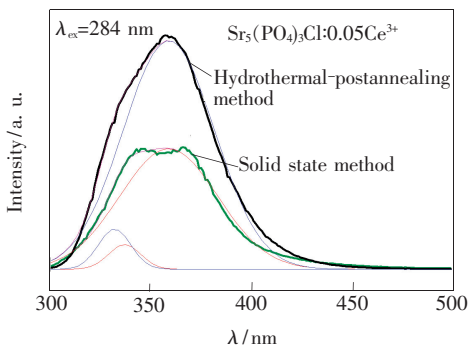

Fig. 11 The emission spectra of $Sr_5(PO_4)_3Cl:Ce^{3+}$ phosphors by two different synthetic methods: Solid-state method and the hydrothermal and post-annealing method involved in present work obtained at calcination temperature of 800 ℃ for 2 h in Ar gas.

Fig. 12 displays two typical chromaticity color coordinates (x, y) of the $Sr_5(PO_4)_3Cl:Ce^{3+}$ phosphors obtained by different methods. The chromaticity color coordinate (0.158 4, 0.023 1) showing in position 1# corresponds to the $Sr_5(PO_4)_3Cl:Ce^{3+}$ phosphor by solid-state method, in which the Ce^{3+} content is 0.05 and calcination temperature is 1 000 ℃. As well, the chromaticity color coordinate (0.165 1, 0.014 1) showing in position 2# corresponds to the $Sr_5(PO_4)_3Cl:Ce^{3+}$ phosphor by the hydrothermal and post-annealing method involved in present work, in which the Ce^{3+} content is 0.05, the solvent composition is pure H_2O and calcination temperature is 800 ℃. Hence, the $Sr_5(PO_4)_3Cl:Ce^{3+}$ phosphors prepared by the hydrothermal and post-annealing method are excellent potential candidate for light-emitting diode devices.

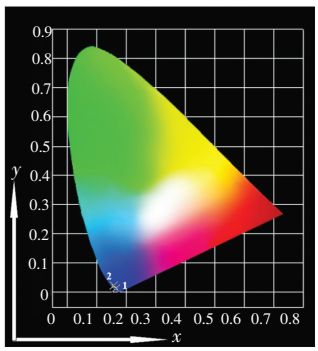

Fig. 12 CIE chromaticity diagram of $Sr_5(PO_4)_3Cl:Ce^{3+}$ phosphors by two different synthetic methods: (1) solid-state method and (2) the hydrothermal and post-annealing method involved in present work (λ_{ex} = 284 nm).

4 Conclusion

We have adopted hydrothermal and post-annealing method to prepare a series of $Sr_5(PO_4)_3Cl:Ce^{3+}$ phosphors. Many experimental parameters affecting the shapes, sizes and PL intensities were emphatically studied. Basically, several scientific merits exist in present work as follows: (1) adding $N_2H_4 \cdot H_2O$ and the reducing gas (Ar-H_2) into solution before hydrothermal treatment can evidently protect the oxidation of Ce^{3+}, which avoid the use of reducing atmosphere during the following post-annealing stage. (2) Rugby-like $Sr_5(PO_4)_3Cl:Ce^{3+}$ nanostructures with various sizes was obtained by hydrothermal treatment, which preferentially grows along [001] direction. (3) The CIE chromaticity coordinates (0.165 1, 0.014 1) illustrates that the as-obtained $Sr_5(PO_4)_3Cl:Ce^{3+}$ phosphors can exhibit excellent emission.

References:

[1] Wang W N, Iskandar F, Okuyama K, *et al*. Rapid synthesis of non-aggregated fine chloroapatite blue phosphor powders with high quantum efficiency [J]. *Adv. Mater.*, 2008, 20(18):3422-3426.

[2] DeLoach L D, Payne S A, Smith L K, *et al*. Laser and spectroscopic properties of $Sr_5(PO_4)_3F:Yb$ [J]. *J. Opt. Soc. Am.* B, 1994, 11(2):269-276.

[3] Kokubo T, Kim H M, Kawashita M. Novel bioactive materials with different mechanical properties [J]. *Acta Biomater.*, 2003, 24(13):2161-2175.

[4] Smet P F, Parmentier A B, Poelman D. Selecting conversion phosphors for white light-emitting diodes [J]. *J. Electro Chem. Soc.*, 2011, 158(6):R37-54.

[5] Guo C, Luan L, Ding X, *et al*. Luminescent properties of $Sr_5(PO_4)_3Cl:Eu^{2+}$, Mn^{2+} as a potential phosphor for UV-LED-based white LEDs [J]. *Appl. Phys.* B, 2009, 95(4):779-785.

[6] Zhang X G, Zhang J L, Gong M L, *et al*. Synthesis and luminescence of Eu^{2+}-doped alkaline-earth apatites for application in white LED [J]. *J. Lumin.*, 2010, 130(4):554-559.

[7] Yu J, Guo C F, Ren Z Y, *et al*. Photoluminescence of double-color-emitting phosphor $Ca_5(PO_4)_3Cl:Eu^{2+}$, Mn^{2+} for near-UV LED [J]. *Opt. Laser Technol.*, 2011, 43(4):762-765.

[8] Dorenbos P. The $4f^n \leftrightarrow 4f^{n-1}$ 5d transitions of the trivalent lanthanidesin halogenides and chalcogenides [J]. *J. Lumin.*, 2000, 91(1/2):91-106.

[9] Lin H H, Liang H B, Su Q, *et al*. Luminescence and site occupancy of Ce^{3+} in $Ba_2Ca(BO_3)_2$[J]. *Phys. Rev.* B, 2007, 76(3):035117-1-8.

[10] Le Toquin R, Cheetham A K. Red-emitting cerium-based phosphor materials for solid-state lighting applications [J]. *Chem. Phys. Lett.*, 2006, 423(4/5/6):352-356.

[11] Jang H S, Jeon D Y. Yellow-emitting $SrM_3SiO_5:Ce^{3+}$,Li^+ phosphor for white-light-emitting diodes and yellow-light-emitting diodes [J]. *Appl. Phys. Lett.*, 2007, 90(4):041906-1-3.

[12] Zeng Q, Liang H B, Su Q, *et al*. Luminescence of Ce^{3+} activated fluoro-apatites $M_5(PO_4)_3F$ (M = Ca, Sr, Ba) under VUV-UV and X-ray excitation [J]. *J. Phys.: Condens. Matter*, 2006, 18(42):9549-9560.

[13] Kottaisamy M, Jagannathan R, Jeyagopal P, *et al*. Eu^{2+} luminescence in $M_5(PO_4)_3X$ apatites, where M is Ca^{2+}, Sr^{2+} and Ba^{2+}, and X is F^-, Cl^-, Br^- and OH^-[J]. *J. Phys.* D: *Appl. Phys.*, 1994, 27(10):2210-2215.

[14] Song Y H, You H P, Zhang H J, *et al*. Facile synthesis and luminescence of $Sr_5(PO_4)_3Cl:Eu^{2+}$ nanorod bundles via a hydrothermal route [J]. *Inorg. Chem.*, 2010, 49(4):1674-1678.

[15] Kannan S, Rocha J H G, Ferreira J M F. Synthesis of hydroxy-chlorapatites solid solutions [J]. *Mater. Lett.*, 2006, 60(7):864-868.

[16] Jevtić M, Mitrić M, Škapin S, *et al*. Crystal structure of hydroxyapatite nanorods synthesized by sonochemical homogeneous precipitation [J]. *Crystal Growth Des.*, 2008, 8(7):2217-2222.

[17] Wang X, Zhuang J, Peng Q, *et al*. Liquid-solid-solution synthesis of biomedical hydroxyapatite nanorods [J]. *Adv. Mater.*, 2006, 18(15):2031-2034.

[18] Ehre D, Cohen H, yahovitskaya V L, *et al*. X-ray photoelectron spectroscopy of amorphous and quasiamorphous phases of $BaTiO_3$ and $SrTiO_3$[J]. *Phys. Rev.* B, 2008, 77(18):184106-1-6.

[19] Zhang Y J, Guan H M. Hydrothermal synthesis and characterization of hexagonal and monoclinic $CePO_4$ single-crystal nanowires [J]. *J. Crystal Growth*, 2003, 256(1-2):156-161.

[20] Rafailov P M, Thomsen C, Dettlaff-Weglikowska U, *et al*. High levels of electrochemical doping of carbon nanotubes: Evidence for a transition from double-layer charging to intercalation and functionalization [J]. *J. Phys. Chem.* B, 2008, 112(17):5368-5373.

[21] Mhin S W, Ryu J H, Kim K M, *et al*. Pulsed-laser-induced simple synthetic route for $Tb_3Al_5O_{12}:Ce^{3+}$ colloidal nanocrystals and their luminescent properties [J]. *Nanoscale Res. Lett.*, 2009, 4(8):888-895.

[22] Shalapska T, Stryganyuk G, Gektin A, *et al*. Crystal structure and luminescence properties of $LiYP_4O1_2:Ce^{3+}$ phosphor [J]. *J. Phys.: Condens. Matter*, 2010, 22(48):485503-1-6.

[23] Liu W R, Huang C H, Chen T M, *et al*. High efficiency and high color purity blue-emitting $NaSrBO_3:Ce^{3+}$ phosphor for

near-UV light-emitting diodes [J]. *J. Mater. Chem.*, 2011, 21:6869-6874.

[24] Dexter D L, Schulman J H. Theory of concentration quenching in inorganic phosphors [J]. *J. Chem. Phys.*, 1954, 22(6):1063-1670.

[25] Lin C C, Lin K M, Li Y Y. Sol-gel synthesis and photoluminescent characteristics of Eu^{3+}-doped Gd_2O_3 nanophosphors [J]. *J. Lumin.*, 2007, 126(2):795-799.

[26] Jung K Y, Lee D Y, Kang Y C, *et al.* Size-dependent luminescent properties of hollow and dense $BaMgAl_{10}O_{17}$:Eu blue phosphor particles prepared by spray pyrolysis [J]. *Korean J. Chem. Eng.*, 2004, 21(5):1072-1080.

[27] Kim T H, Kang S H. Hydrothermal synthesis and photoluminescence properties of nano-crystalline $GdBO_3$:Eu^{3+} phosphor [J]. *Mater. Res. Bull.*, 2005, 40(11):1945-1954.